Supporting Information

Large-scale synthesis of ultrathin tungsten oxide nanowire networks: an efficient catalyst for aerobic oxidation of Toluene to Benzaldehyde under Visible Light

Experimental Section

Synthesis of $W_{18}O_{49}$ ultrathin nanowire networks. In a typical procedure, 2 g of WCl_6 and 4 ml of hydrofluoric acid (30% m/m) was dissolved in a mixture of 200 mL of ethanol and isooctanol, and the obtained blue suspension was magnetically stirred for 2 h, and then transferred to a teflon–lined stainless–steel autoclave and heated at 180 °C for 20 h with a heating rate of 4 °C/min. The autoclave was cool down naturally and a blue product was collected, washed, and dried in air.

Photocatalytic Toluene Oxidation. The photocatalytic activity of the $W_{18}O_{49}$ ultrathin nanowires was evaluated by preparation of benzaldehyde from toluene catalyzed oxydation under visible light ($\lambda \geq 420$ nm) irradiation from a 300W Xe lamp (HSX-F300, NBeT). The photocatalyst (50 mg) was poured into 10 mL benzene (contains 30 μL of toluene) in a sealed quartz reactor at room temperature. Before light was turned on, the suspension was continuously stirred for 30 min in dark to ensure the establishment of an adsorption–desorption equilibrium. The concentration of benzaldehyde during the photocatalytic process was monitored by colorimetry using a gas chromatography-mass spectrometry (Agilent 6890/5975 GC-MS, USA).

Activity Recovery. After photochemical reaction, the nanowire sample was loaded into $NaBH_4$ aqueous solution (0.1 M) under stirring, the colour of the suspension was gradually changed from yellow-green to blue. After 1h, the blue products were collected, purified with absolute and distilled water, and dried in vacuum at 50 °C.

Characterization. XRD patterns of the products were recorded on a Bruker D8 Focus

diffractometer by using CuKα radiation (λ = 1.54178 Å). Scanning electron microscopy (SEM) images and EDS spectrums were obtained on a Hitachi S–4800. Transmission electron microscopy (TEM) and high–resolution TEM (HRTEM) characterizations were performed with a Tecnai G F30 operated at 300 kV. UV–Vis–NIR absorption spectra were recorded with a Shimadzu UV-3600. X-ray Photoelectron Spectroscopy (XPS) experiments were performed in a Theta probe (Thermo Fisher) using monochromated Al Kα X-rays at hυ = 1486.6 eV. Peak positions were internally referenced to the C1s peak at 284.6 eV. Fourier transform infrared (FTIR) spectra were obtained from THERMO Iz10. BET measurements were carried out in Micromeritics Tristar 3000.

Computation Details. All the DFT calculations were carried out using the Vienna ab initio simulation package (VASP).[1-3]The energy cutoff for the plane wave basis set was 600eV. The generalized gradient approximation (GGA) with the function of Perdew and Wang (PW91)[4] was used to deal with the exchange correlation energies. And the electron-ion interaction was described by the projected augmented wave (PAW) method.[5,]For the bulk calculation, the geometry optimization was stopped when force on each atom was less than 0.01 eV/Å. Brillouin zones were sampled with Monkhorst-Pack k-points of 4x4x4, 2x10x3 for WO_3 and $W_{18}O_{49}$, respectively. The optimized lattice constants of bulk are compiled in Table1, in reasonable agreement with the experimental and calculated values.[7-9]

The Brillouin zone sampling was carried out with the k-points of 1 x 5 x 1 for the $W_{18}O_{49}$ nanowire calculation. The atomic relaxation was stopped until the force on

each atom was smaller than 0.05 eV/Å as previous report.[7]A larger 1x15x1 k-point was used for the calculations of density of states (DOS) at the DFT level. Note that pure DFT always underestimates the band gaps in comparison with the experimental values, so a hybrid functional approach implemented in the framework of Heyd-Scuseria-Ernzerh of (HSE06)[10-12] is used to obtain the electronic structuresof the WO_3 and $W_{18}O_{49}$ nanowires. It is found that when using 45% (i.e, mixing parameter α=0.45)mixing of HF, a direct band gap of 2.83eV was obtained for the WO_3 bulk, which is well consistent with the experimental gap of 2.6-3.2eV.[13-15] So this parameter is also used in the calculation of the $W_{18}O_{49}$ nanowires.

(1) Kresse, G.; Hafner, J. *Physical Review B* **1994**, *49*, 14251.

(2) Kresse, G.; Furthmüller, J. *Computational Materials Science* **1996**, *6*, 15.

(3) Kresse, G.; Furthmüller, J. *Physical Review B* **1996**, *54*, 11169.

(4) Perdew, J. P.; Chevary, J. A.; Vosko, S. H.; Jackson, K. A.; Pederson, M. R.; Singh, D. J.; Fiolhais, C. *Physical Review B* **1992**, *46*, 6671.

(5) Blöchl, P. E. *Physical Review B* **1994**, *50*, 17953.

(6) Kresse, G.; Joubert, D. *Physical Review B* **1999**, *59*, 1758.

(7) Migas, D. B.; Shaposhnikov, V. L.; Borisenko, V. E. *The Journal of Apply Physics* **2010**, *108*, 093714.

(8) Valdes, A.; Kroes, G. J. *The Journal of chemical physics* **2009**, *130*, 114701.

(9) Wang, F.; Di Valentin, C.; Pacchioni, G. *The Journal of Physical Chemistry C* **2012**, *116*, 8901.

(10) Heyd, J.; Scuseria, G. E.; Ernzerhof, M. *The Journal of chemical physics* **2003**,

118, 8207.

(11) Heyd, J.; Scuseria, G. E. *The Journal of chemical physics* **2004**, *121*, 1187.

(12) Heyd, J.; Scuseria, G. E.; Ernzerhof, M. *The Journal of chemical physics* **2006**, *124*, 219906.

(13) Niklasson, G. A.; Granqvist, C. G. *The Journal of Material Chemistry* **2007**, *17*, 127.

(14) Zheng, H.; Ou, J. Z.; Strano, M. S.; Kaner, R. B.; Mitchell, A.; Kalantar-zadeh, K. *Advance Function Materials* **2011**, *21*, 2175.

(15) Vemuri, R. S.; Engelhard, M. H.; Ramana, C. V. *ACS applied materials & interfaces* **2012**, *4*, 1371.

Supporting Figures

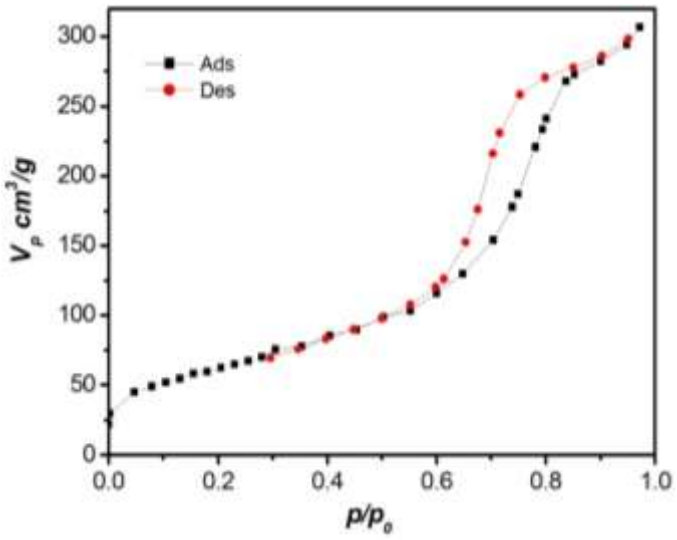

Figure S1. Nitrogen adsorption–desorption isotherm plot of the as-synthesized $W_{18}O_{49}$ ultrathin nanowire networks.

Figure S2. Photograph of the as-prepared $W_{18}O_{49}$ ultathin nanowire networks.

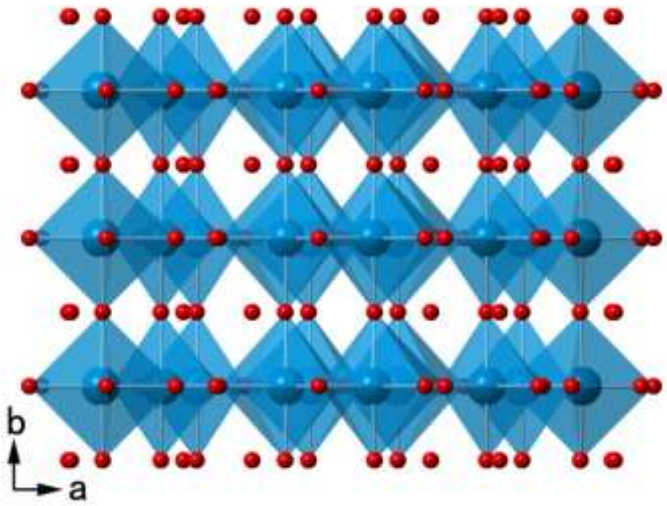

Figure S3. Crytal structure of the monoclinic phase $W_{18}O_{49}$.

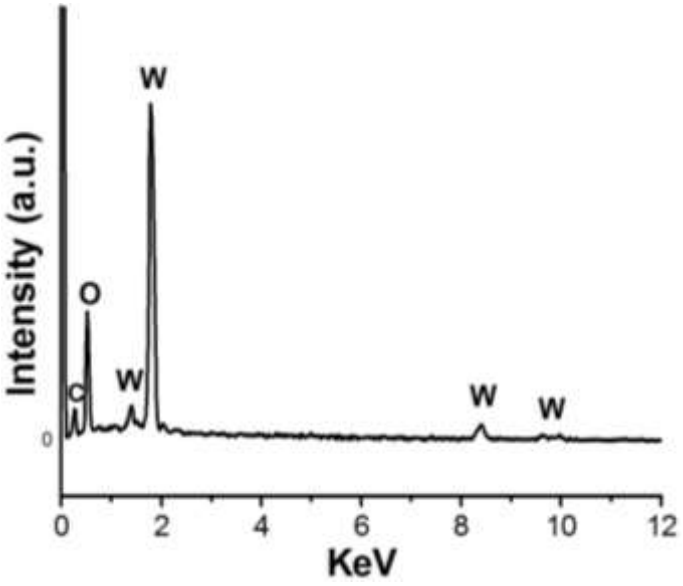

Figure S4. EDS spectrum of the as-synthesized ultrathin $W_{18}O_{49}$ nanowire networks.

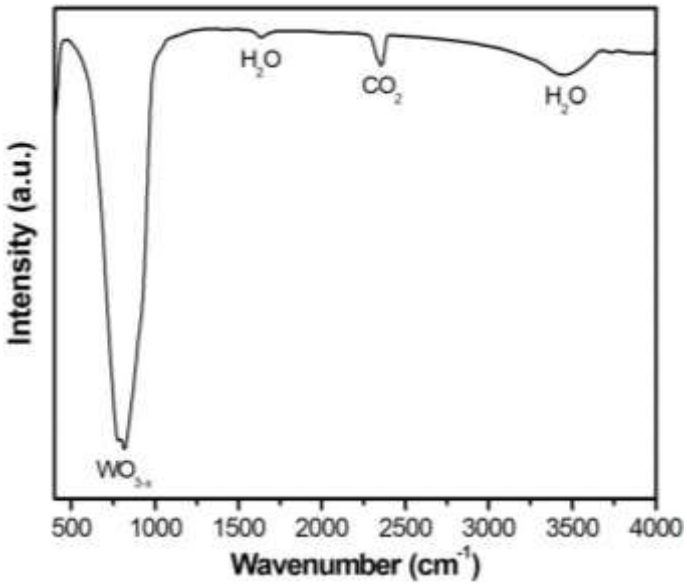

Figure S5. FTIR spectrum of the as-synthesized $W_{18}O_{49}$ ultrathin nanowire networks.

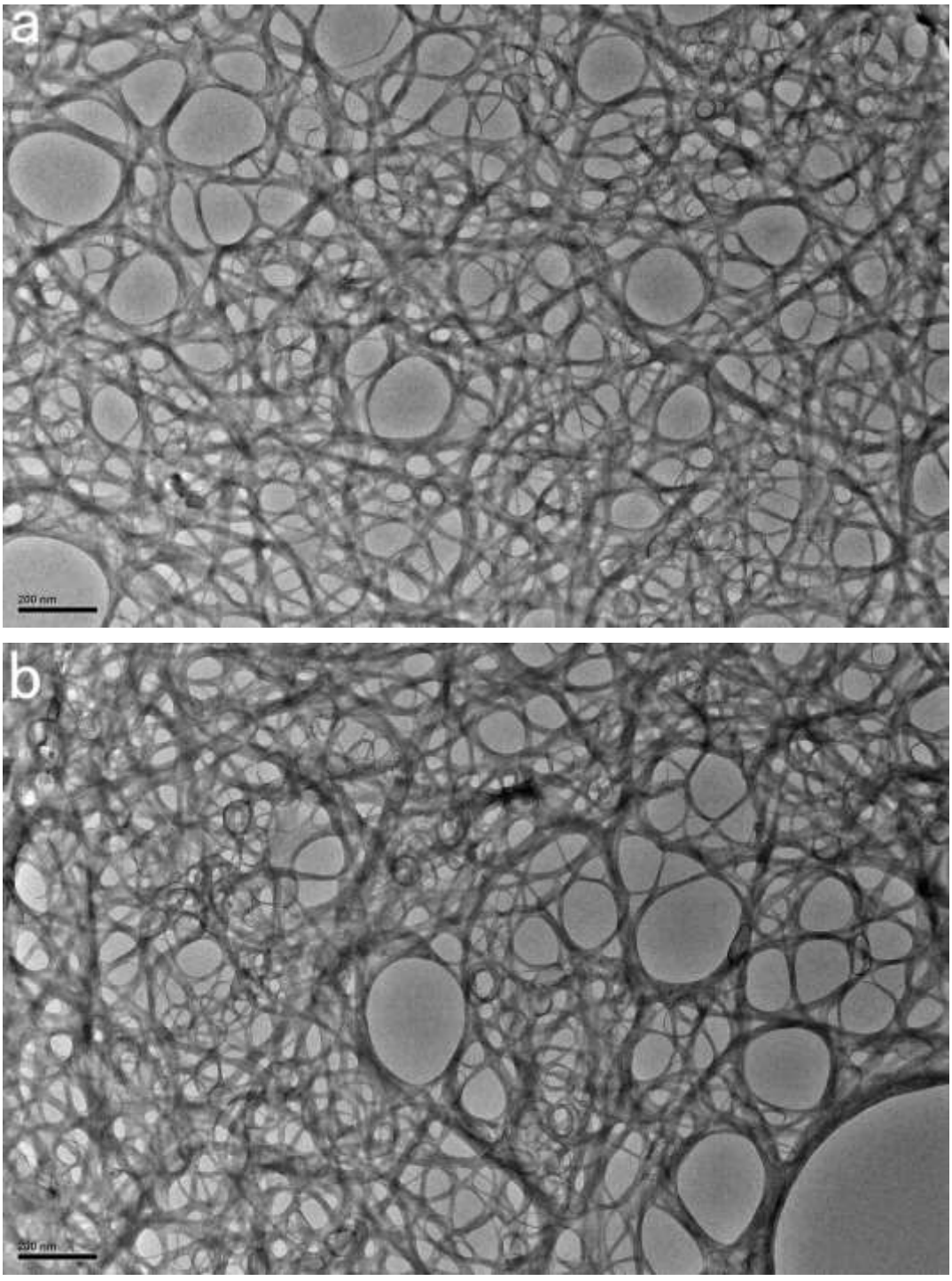

Figure S6. Two typical low-magnification TEM images of the $W_{18}O_{49}$ nanowire networks.

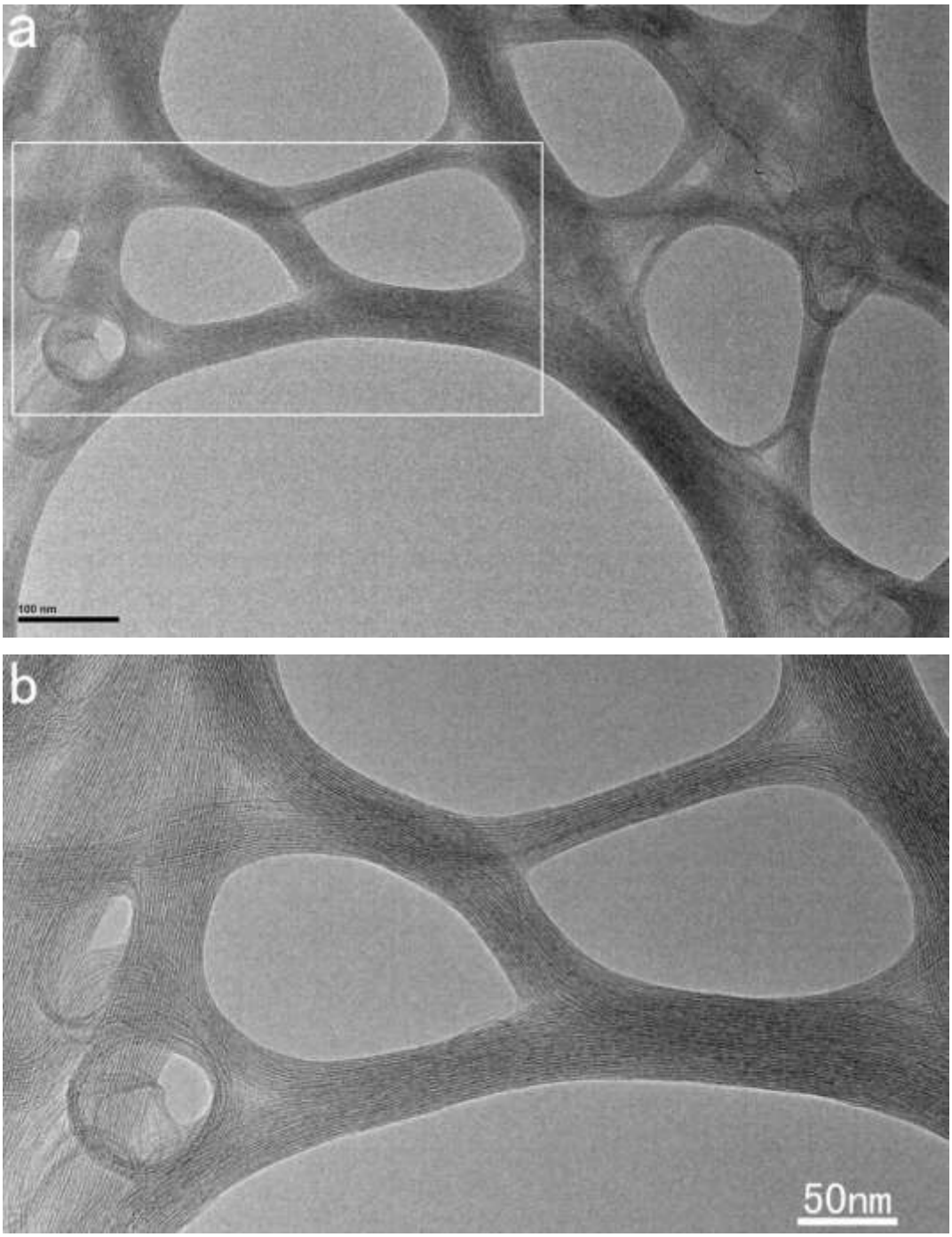

Figure S7. High-magnification TEM images of the $W_{18}O_{49}$ ultrathin nanowire networks.

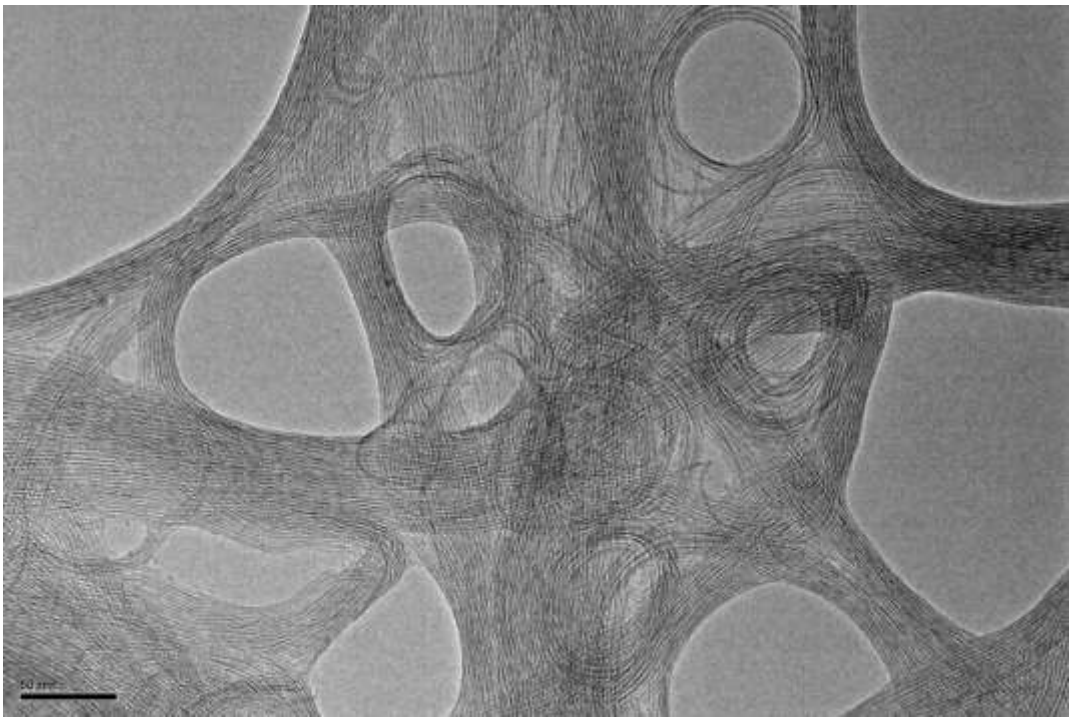

Figure S8. The as-synthesized $W_{18}O_{49}$ ultrathin nanowires with remarkable flexibility.

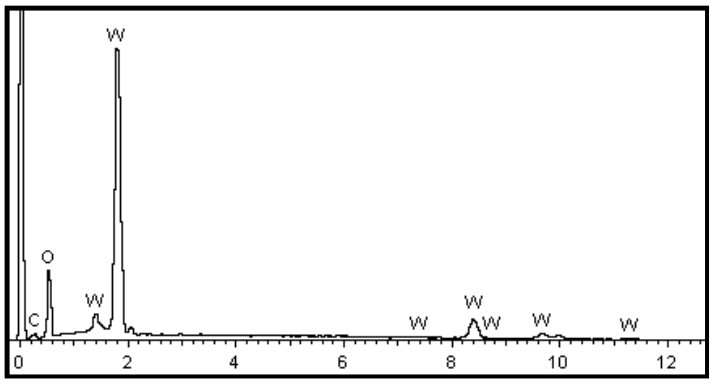

Figure S9. EDS spectrum of the as-synthesized ultrathin $W_{18}O_{49}$ nanoparticles prepared at 180 °C for 4 h.

Figure S10. TEM image of the $W_{18}O_{49}$ ultrathin nanowire networks obtained after 20 h reaction.

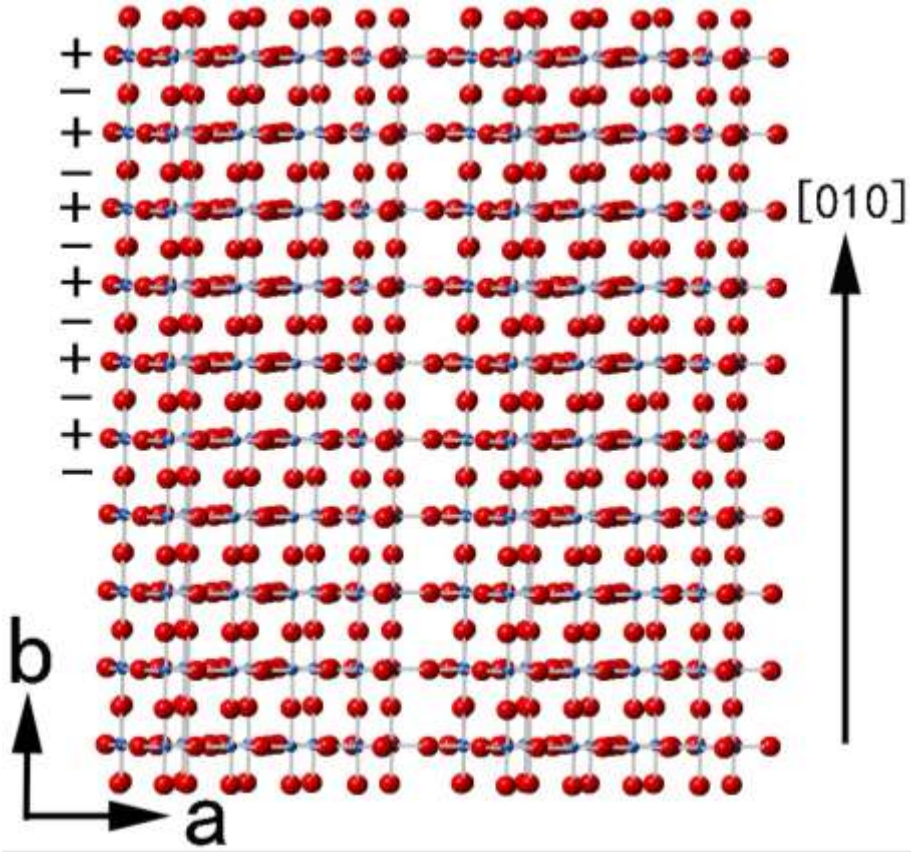

Figure S11. Polar surfaces in the crystal structure of monoclinic phase $W_{18}O_{49}$.

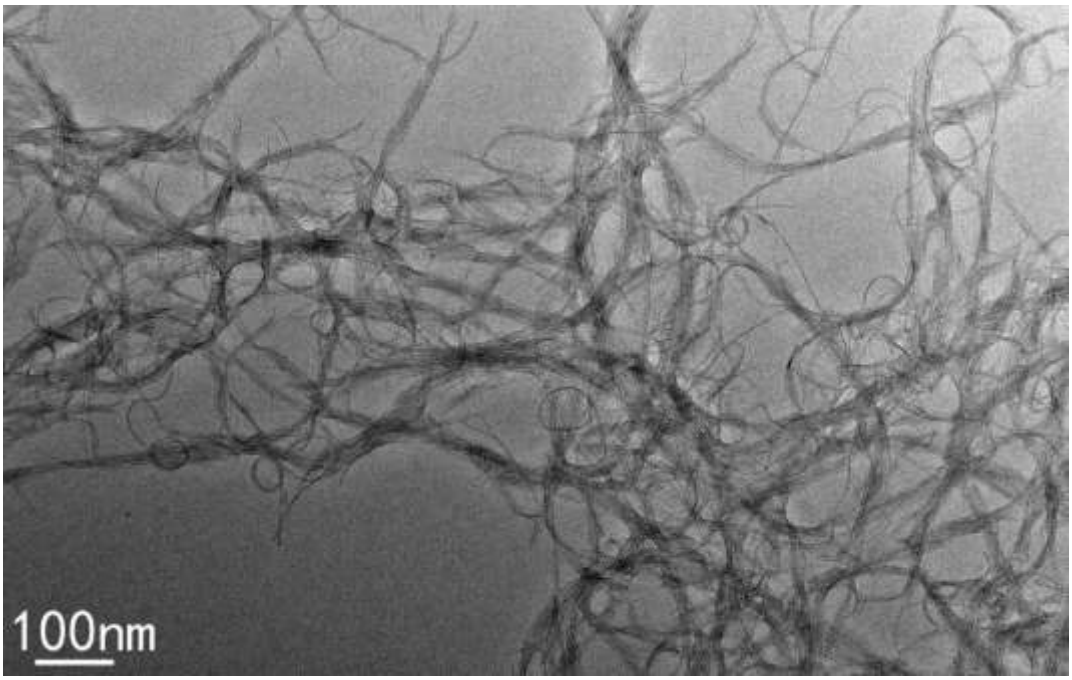

Figure S12. TEM image of the dispersed $W_{18}O_{49}$ ultrathin nanowires prepared when HF was not added into the reaction precursors.

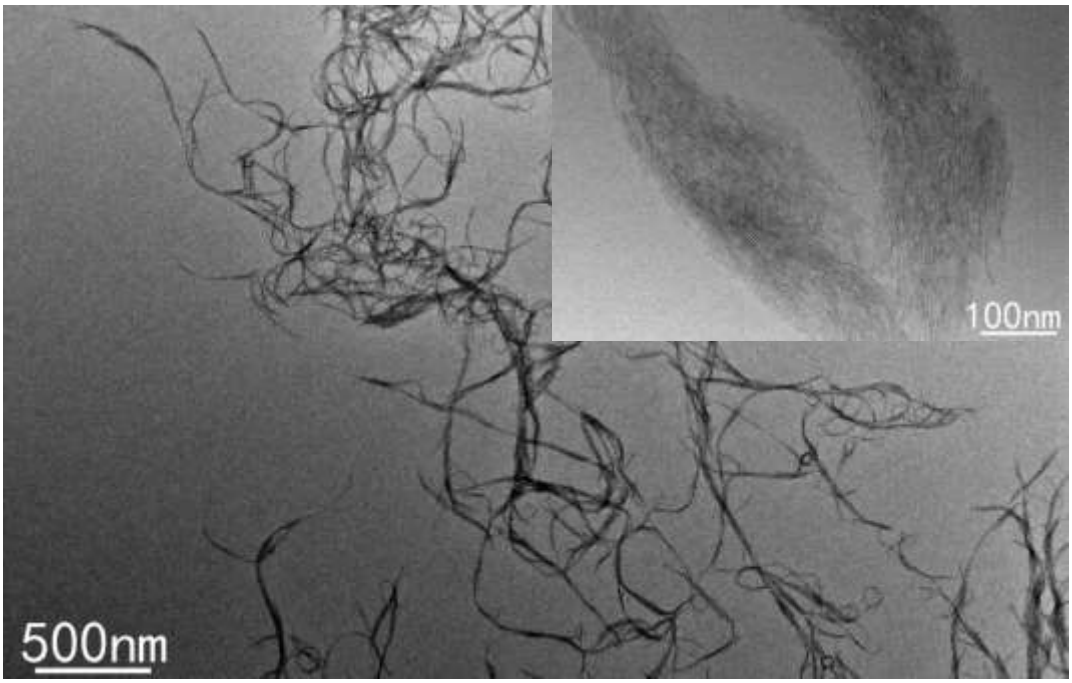

Figure S13. TEM image of the long $W_{18}O_{49}$ ultrathin nanowire bounds prepared when the volume ratio of ethanol to isooctanol is 4.

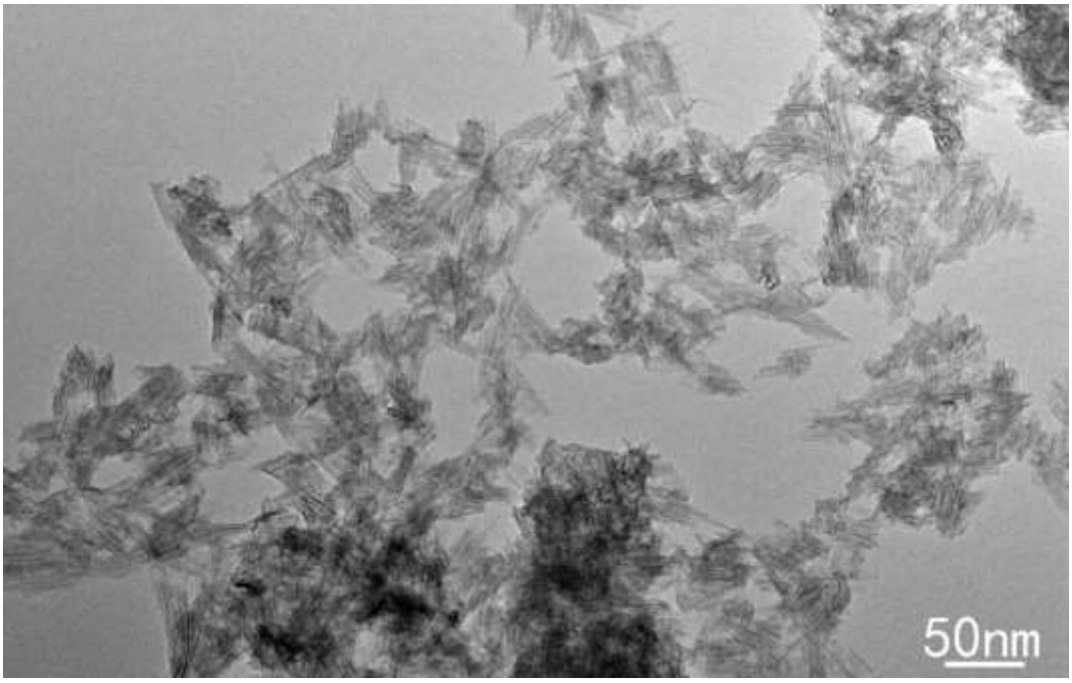

Figure S14. TEM image of the short $W_{18}O_{49}$ ultrathin nanowire bounds prepared when the volume ratio of ethanol to isooctanol is 0.25.

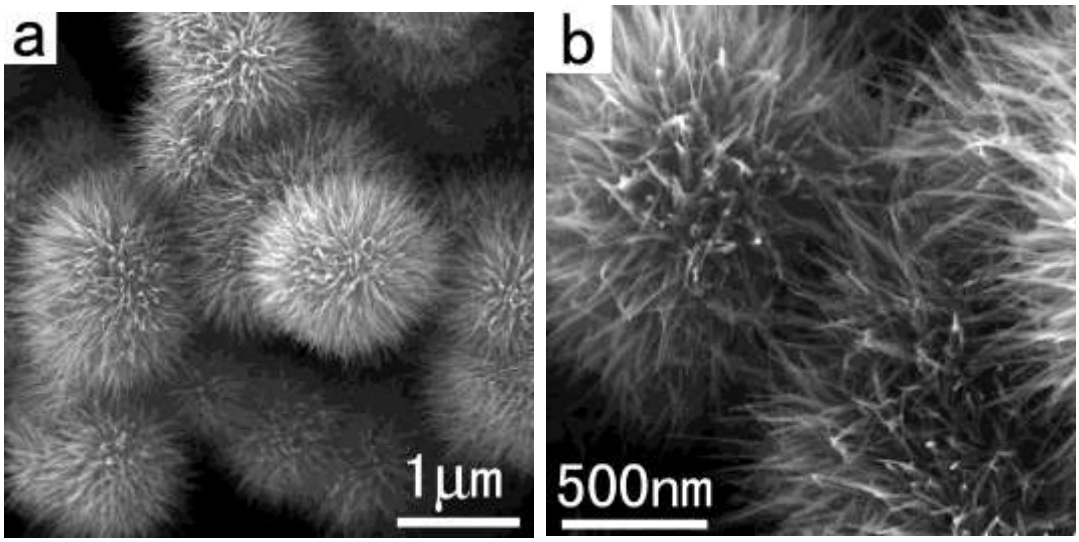

Figure S15. SEM images of the 3D urchin-like nanowires with larger diameters (5-7 nm) prepared when the C_{WCl6} = 1.5 g/100 mL.

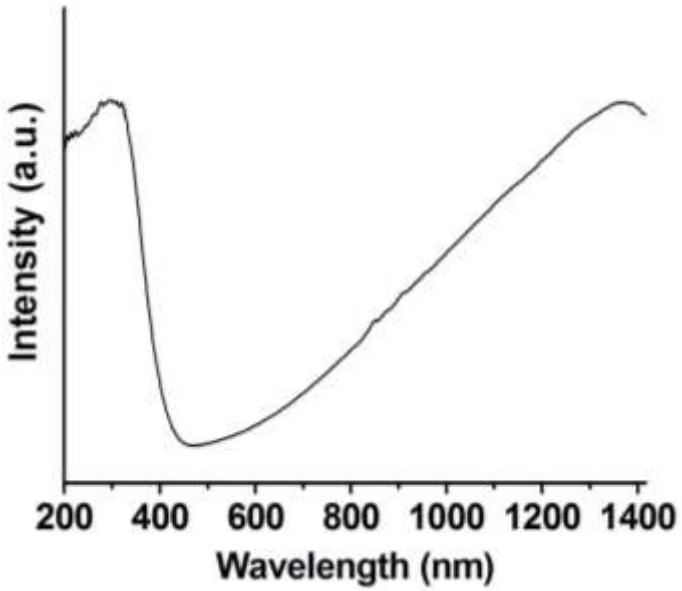

Figure S16. UV-Vis-NIR absorption spectrum of the dispersed $W_{18}O_{49}$ ultrathin nanowires shown in Figure S12.

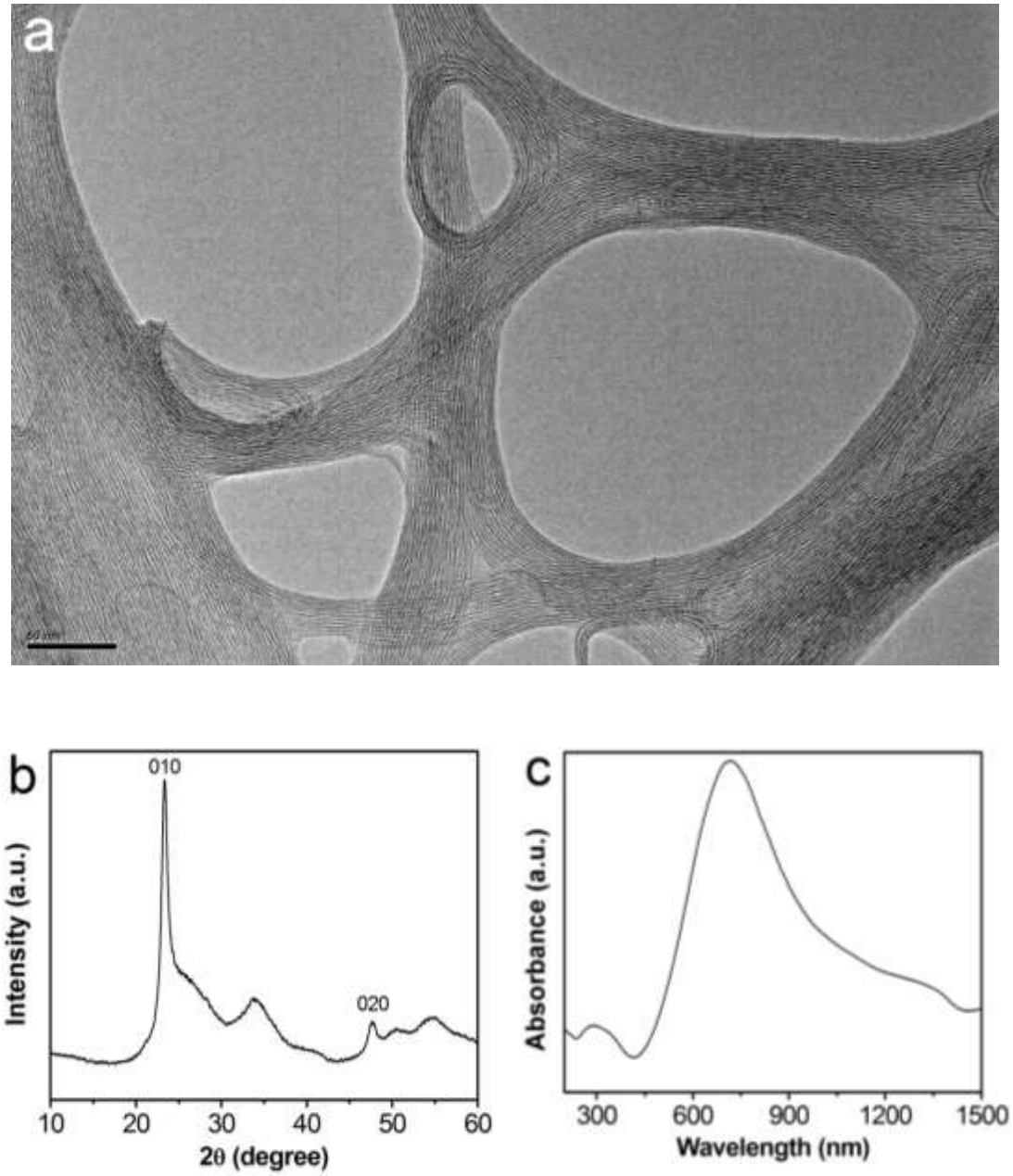

Figure S17. TEM image (a), XRD pattern (b), and UV/Vis-NIR spectrum (c) of the tungsten oxide catalysts after reaction.

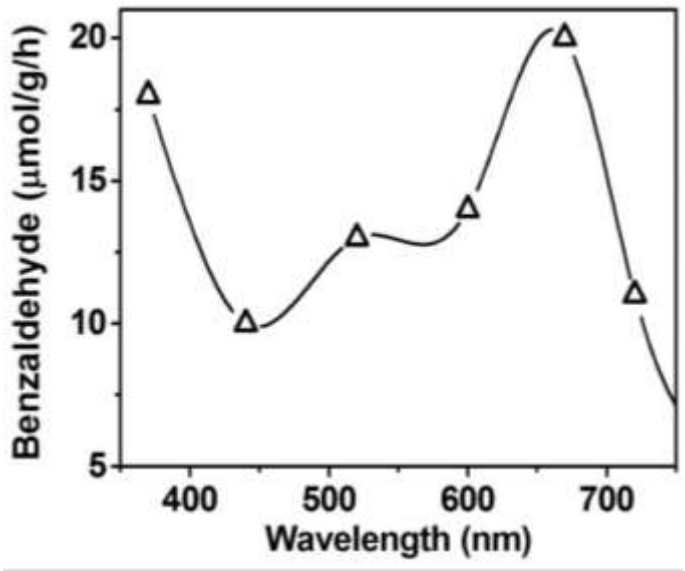

Figure S18. Wavelength-dependent benzaldehyde evolution with the $W_{18}O_{49}$ ultrathin nanowires as photocatalysts.

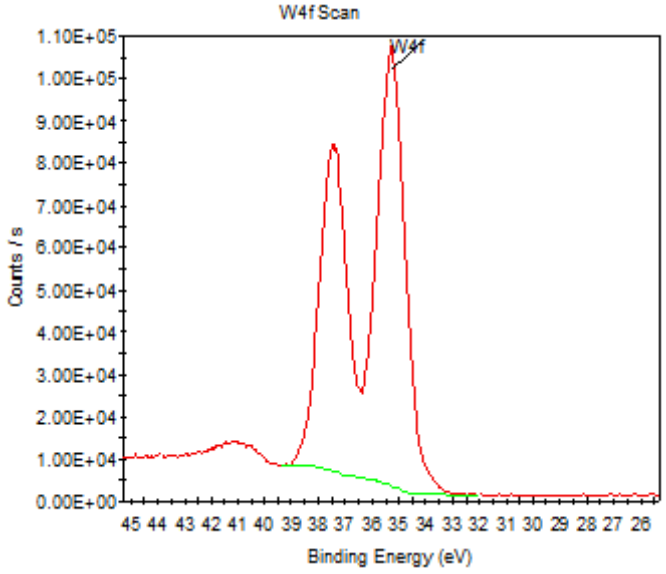

Figure S19. XPS spectrum of the sample W-300-8 min. The two peaks can be well indexed with the W4f of W^{6+}.

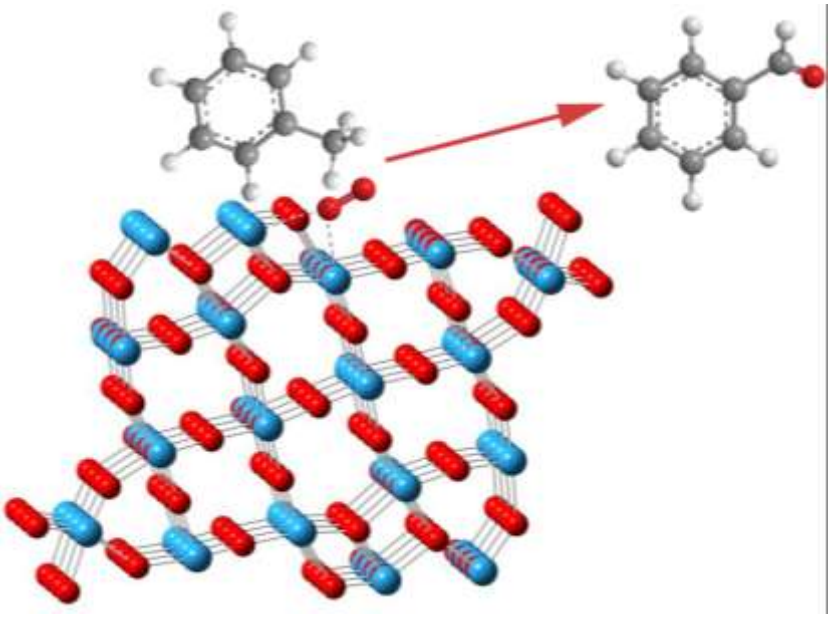

Figure S20. schematic illumination of the “trap” effect results from the oxygen vacancies in the photocatalytic reaction.